
Article:
Derrat, H.S. orcid.org/0000-0002-8662-7917, Robertson, C.C. orcid.org/0000-0002-1419-9618, Meijer, A.J.H.M. orcid.org/0000-0003-4803-3488 et al. (1 more author) (2018) Turning intercalators into groove binders: synthesis, photophysics and DNA binding properties of tetracationic mononuclear ruthenium(ii)-based chromophore-quencher complexes. Dalton Transactions, 47 (35). pp. 12300-12307. ISSN 1477-9226

https://doi.org/10.1039/c8dt02633e

Journal Name

Dynamic Article Links ►

Cite this: DOI: 10.1039/c0xx00000x

www.rsc.org/xxxxxx

ARTICLE TYPE

Turning intercalators into groove binders: synthesis, photophysics and DNA binding properties of tetracationic mononuclear Ruthenium(II)-based chromophore-quencher complexes

Hanan S Derrat,[a,b] Craig C. Robertson,[a] Anthony JHM Meijer,[a] and Jim A Thomas*[a]

Received (in XXX, XXX) Xth XXXXXXXXX 20XX, Accepted Xth XXXXXXXXX 20XX
DOI: 10.1039/b000000x

The synthesis of two new tetracationic mononuclear Ru^{II} complexes containing the tetrapyridyl [3,2-a:2',3'-c:3",2"-h:2"',3"'-j] phenazine ligand in which the uncoordinated site has been converted into a dicationic ethylene-bipyridyldiylium unit is reported. The structure of the complexes is fully assigned through detailed NMR studies and, in one case, through an X-ray crystallography study. Voltammetry, optical spectroscopy and computational studies confirm that the bipyridyldiylium moiety has a low-lying reduction that quenches the ^{3}MLCT-based emission usually observed in such systems. The new complexes interact with DNA in a quite different manner to their dicationic analogues: they both bind to duplex DNA with micromolar affinity through groove binding. These observations are rationalized through a consideration of their structural and electronic properties.

Introduction

Due to their potential as therapeutics, small molecules that bind to DNA are much studied. Although originally focused solely on organic systems, [1-4] the discovery that cisplatin is genotoxic due to irreversible DNA binding[5-7] led to such research being extended to a range of metal complexes. In the last two decades, metal complexes that reversibly interact with DNA have been increasingly investigated. Much of this latter work has centred on photo-excitable transition metal centres and, *inter alia*, this has led to the identification and development of systems that can cleave DNA site and sequence selectively, as well as luminescence-based imaging probes. [8-10] Many luminescent systems are based on the intercalating Ru^{II}(dppz) moiety (dppz = dipyrido [3,2-a:2',3'-c] phenazine) as this leads to a "light-switch" effect in which Ru^{II} →dppz ^{3}MLCT emission is only switched on through intercalation. [11-17]

In several previous studies we have investigated systems that interact with DNA through less studied motifs. This work has identified several high-affinity, groove-binding complexes that display good selectivity and novel optical outputs.[18,19] We have also described self-assembled oligonuclear macrocycles that bind to duplex DNA through a unique external mode[20,21] and function as novel sensitizers for photodynamic therapy.[22] We have also reported on non-classical intercalating metal complexes which - despite containing unfused polyaromatic ring systems more characteristic of groove binders - are confirmed intercalators.[23] Comparisons between almost structurally identical complexes, revealed that intercalation could be switched to groove binding through subtle changes to the electronic distribution within a system.

Apart from investigating the DNA binding properties of such complexes - we have also studied purely organic cations based on dppz and analogues, and found that they bind to duplex DNA with affinities that are comparable to many metal complexes and possess highly energetic excited states capable of inducing redox damage to nucleobase sites.[24,25] Herein we describe the synthesis, and photophysical and biophysical properties of tetracationic metal complexes that incorporate features of both architectures by containing an intercalating cation site coordinated to a Ru^{II} center. These studies have revealed that, despite incorporating extended rigid and virtually flat polyaromatic ligands characteristic of classical intercalators, these newly reported complexes are in fact also groove binders.

Results and Discussion

Synthesis and characterization

After the tpphz-based (tpphz = tetrapyridyl [3,2-a:2',3'-c:3",2"-h:2"',3"'-j] phenazine) complexes $\mathbf{1}^{2+}$ and $\mathbf{2}^{2+}$ - Figure 1 - were synthesized using reported methods,[26,27] quaternization of their free "phen" site of tpphz to create a pendent ethylene-bipyridyldiylium unit was investigated. After numerous unsuccessful attempts, this aim was finally achieved by refluxing the complexes for 8 days in dibromoethane. The resultant precipitates of [**3**]Br_4 and [**4**]Br_4 were collected, converted to hexafluorophosphate salts, and then purified by column chromatography.

Studies by Bolger, *et al.* demonstrated that the proton NMR spectra of [**1**]$(PF_6)_2$ in acetonitrile is concentration dependent: due to aggregation of cations driven by π-stacking, large downfield shifts in the tpphz-based protons of the complex are observed as its concentration is increased.[28] Contrastingly, the

proton NMR spectra of $\mathbf{3}^{4+}$ and $\mathbf{4}^{4+}$ show no concentration dependence; presumably the additional cationic charge of the terminal ethylene-bipyridyldiylium moieties within the quaternized tppz units suppresses stacking of these complexes in solution.

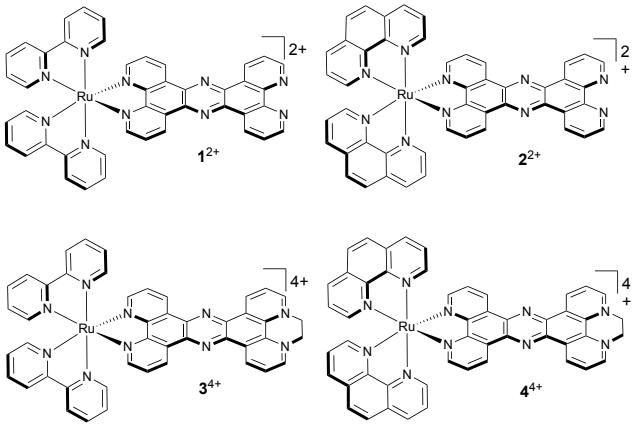

Fig 1. Structures of complexes relevant to this report.

The proton NMR spectra of both complexes as hexafluorophosphate salts were fully assigned through comparisons with related systems and with the aid of COSY and GOESY (Gradient enhanced nuclear Overhauser effect spectroscopy) techniques.

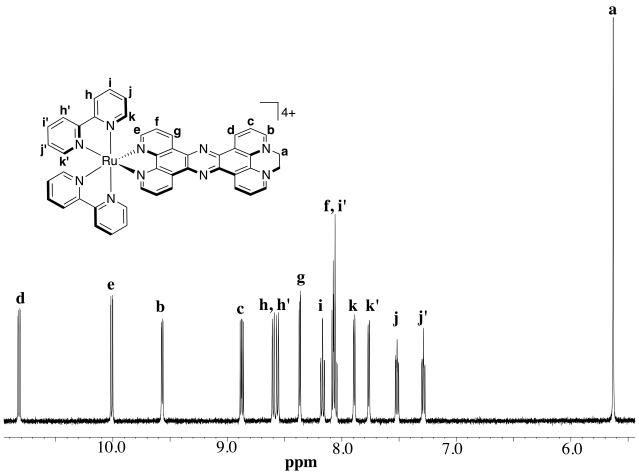

Fig 2 Details of the ^{1}NMR spectrum of $[\mathbf{3}](PF_6)_4$ in acetonitrile.

For example, in the spectrum of $\mathbf{3}^{4+}$ a singlet at ~5.65 ppm that integrates for four protons is assigned to the ethylene bridged protons (**a**) – Figure 2. The GOESY spectrum of this complex shows coupling between (**a**) and a doublet at 9.57 ppm, which is therefore assigned as protons (**b**). In turn, protons (**b**) are cross coupled to the multiplet at 8.05 ppm which itself is cross coupled to the doublet at 10.84; therefore these two signals are assigned to (**c**) and (**d**) respectively. Since (**e**) is rendered inequivalent due to its coordination to ruthenium it is assigned to the resonance at 10.03 ppm, which is cross-coupled to the multiplet at 8.05ppm, assigned to protons (**f**). The bpy-based signals were assigned through a similar analysis. For example, resonances at 7.90 ppm and 7.75 ppm, assigned to proton **(k)** and **(k`),** respectively, are cross-coupled to signals as 7.50 ppm and 7.25ppm, which themselves are thus assigned to **(j)** and **(j')** respectively. Protons **(j)** and **(j')** are also cross-coupled to signals at 8.05 and 8.15 ppm and Through an analogous analysis the somewhat simpler spectrum of $\mathbf{4}^{4+}$ was also fully assigned.

Crystallography Studies.

The structure of $[\mathbf{3}](PF_6)_4$ was further confirmed by single crystal X-ray diffraction studies. Suitable single crystals were grown through vapour diffusion of diethyl ether into acetonitrile solutions of $[\mathbf{3}](PF_6)_4$ and although the quality of the resultant data is relatively low (R_1 = 15.18%), the formulation and connectivities of the cation are confirmed. As for many other complexes that are potentially capable of intercalating into DNA, extensive stacking between the extended aromatic ligands of the cations is observed within the structure - Figure 3.

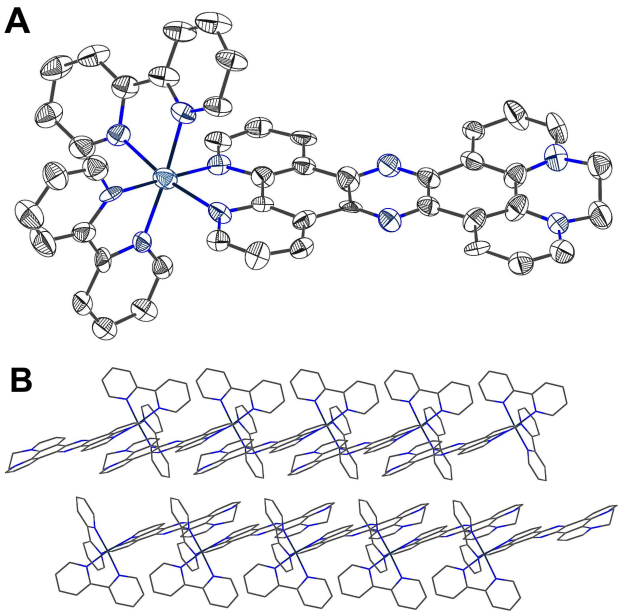

Fig 3. (A) X-ray crystal structure of cation of $[\mathbf{3}](PF_6)_4$ (B) Extended stacking interactions observed in structure. To facilitate visualization, hydrogen atoms, counter-ions and solvent molecules have been removed from these images.

Electrochemical studies.

Cyclic voltammograms of complex **[3]**$[(PF_6)_4]$ and complex **[4]**$[(PF_6)_4]$ were performed at a scan rate of 200 mV s^{-1} at 25°C in acetonitrile solution containing 0.1 M tetra butylammonium hexafluoro phosphate (TBAP), as the supporting electrolyte, under a nitrogen atmosphere.

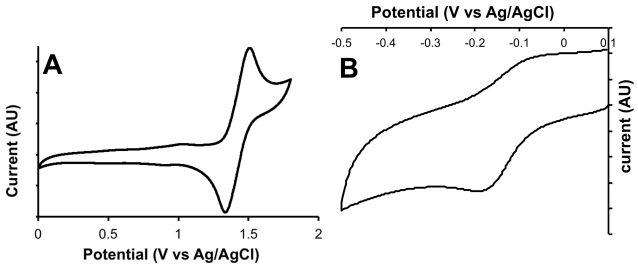

Fig 4. Details of the cyclic voltammogram of $[\mathbf{3}](PF_6)_4$ in acetonitrile. (A) oxidation couple. (B) First reduction couple.

The metal-based oxidations of the complexes are similar to the parent complexes **1** and **2**,[28] as they both display typical reversible $Ru^{II/III}$-based oxidations – Fig 4, Table 1. However, their reductions display a striking new feature: an electrochemically reversible low lying couple at -0.15 V that is observed in related organic cations[29] and is characteristic of the ethylene-bipyridyldiylium moiety, confirming that the uncoordinated nitrogen sites on the tpphz ligand have been quaternized.

Table 1. Summary of the electrochemical properties of [**3**]$(PF_6)_4$ and [**4**]$(PF_6)_4$ (vs. Ag^+/AgCl)

Complex[a]	Oxidation $E_{1/2}$ (V)	Reduction E_p (V)
$\mathbf{3}^{4+}$	+1.40	-0.15, -1.39[a], -1.75[a]
$\mathbf{4}^{4+}$	+1.25	-0.15, -1.15[a],-1.59[a]

[a]chemically irreversible couples hence Ep quoted

Optical Spectroscopy.

Comparisons of the high energy transitions within the absorption spectra of **1** – **4** reveal a great deal of similarity with, for example, intense bands between 200 -300 nm due to ligand-centred $\pi \rightarrow \pi^*$ transitions and lower energy ^{1}MLCT transitions being observed. However, differences - particularly at lower energies - are apparent.

In contrast to $\mathbf{1}^{2+}$ and $\mathbf{2}^{2+}$, which both display separate, characteristically structured, tpphz centered bands between 350 and 400 nm and unstructured Ru→L ^{1}MLCT bands at 400-500 nm, complexes $\mathbf{3}^{4+}$ and $\mathbf{4}^{4+}$ display a single, much broader, unstructured band that stretches out beyond 600 nm – see the following section for more details.

More striking differences between the complexes are observed in emission properties. Unlike, $\mathbf{1}^{2+}$ and $\mathbf{2}^{2+}$, which display unstructured Ru→tpphz ^{3}MLCT based emission in MeCN, neither $\mathbf{3}^{4+}$ nor $\mathbf{4}^{4+}$, display any luminescence. This observation - which is consistent with studies on related systems containing easily reduced ligands - indicates the ^{3}MLCT excited state is quenched through electron transfer to the terminal diquaternary moiety of the extended ligand. As outlined in the following section this hypothesis is also consistent with computational studies.

DFT studies

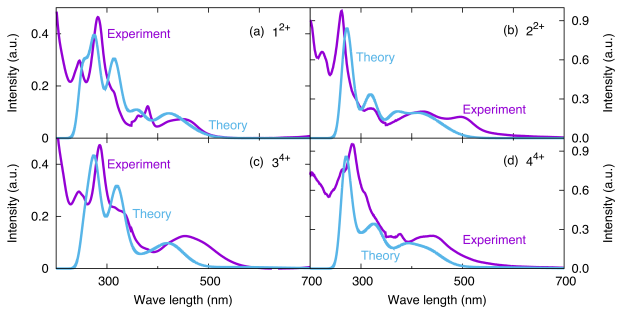

Fig 5. DFT calculated UV-VIS spectra of $\mathbf{1}^{2+}$ [panel (a)], $\mathbf{2}^{2+}$ [panel (b)], $\mathbf{3}^{4+}$ [panel (c)], and $\mathbf{4}^{4+}$ [panel (d)] in acetonitrile. Blue indicates theory, purple indicates experimental data.

DFT optimizations and TD-DFT calculations were performed as described in the experimental section. The resultant structures and coordinates are available in the supporting information. Our TD-DFT calculations show that the agreement between theory and experiment is semi-quantitative with the main features in the absorption spectra for each of the complexes reproduced in the calculations (see Figure 5).

The DFT calculations also confirm the nature of the triplet excited states. Figure 6 shows the spin density for the triplet state for each of the complexes. The spin densities clearly show that for both $\mathbf{1}^{2+}$ and $\mathbf{2}^{2+}$ the excitation is from a metal-centred orbital into an orbital located largely on the phen part of the tpphz ligand, as is expected for the observed Ru→tpphz ^{3}MLCT based excited state. On the other hand, for $\mathbf{3}^{4+}$ and $\mathbf{4}^{4+}$ the excitation is clearly into an orbital located on the "diquat" region of the cation. This is consistent with the experimental studies and confirms that the excited state of the new complexes leads to charge separated states.

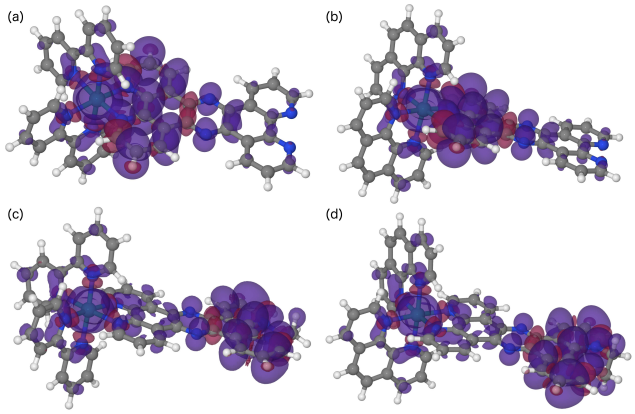

Fig 6. DFT calculated spin densities for the lowest triplet state of $\mathbf{1}^{2+}$ [panel (a)], $\mathbf{2}^{2+}$ [panel (b)], $\mathbf{3}^{4+}$ [panel (c)], and $\mathbf{4}^{4+}$ [panel (d)] in acetonitrile. Blue indicates α-density, red indicates β-density.

DNA binding studies.

Previously reported studies on $\mathbf{1}^{2+}$ and $\mathbf{2}^{2+}$ have conformed that these complexes bind to duplex DNA with high affinities through intercalation.[27,30] In this context, the DNA binding properties of [**3**]Cl_4 and [**4**]Cl_4 were also investigated. Addition of CT-DNA to aqueous buffer solutions of either of the new complexes produced characteristic changes in the absorption spectra. In particular, the low energy bands such as the MLCT transition show distinct hypochromicity, Figure 6, which is typically seen when such metal complexes interact with DNA.

By fitting the changes in the MLCT band to the non-cooperative McGhee-von Hippel model for binding to an isotropic lattice,[31] the estimates of binding parameters summarized in Table 2 were obtained. To aid comparisons the previously reported data for $\mathbf{1}^{2+}$ and $\mathbf{2}^{2+}$ are also included.

Interestingly, although $\mathbf{1}^{2+}$ and $\mathbf{2}^{2+}$ have quite different binding properties, those of complexes $\mathbf{3}^{4+}$ and $\mathbf{4}^{4+}$ are quite similar to each other; both display high affinity micromolar binding and site sizes that are slightly lower than those expected for intercalators. Nevertheless, site sizes such as these are often observed and usually attributed to additional external binding onto the duplex.[32]

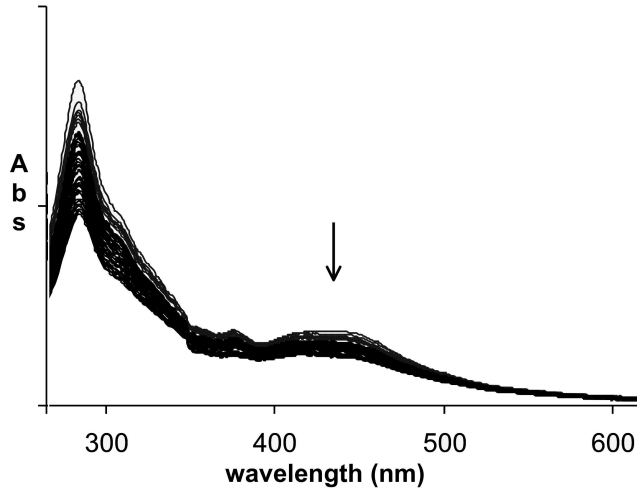

Fig. 7. Details of changes in absorptions spectrum on of complex [**3**]Cl_4 on progressive addition of CT-DNA (5 mM TRIS, 25 mM NaCl, pH 7.0 at 25°C).

The fact that $\mathbf{3}^{4+}$ and $\mathbf{4}^{4+}$ have very similar binding affinities, which are between the values reported for $\mathbf{1}^{2+}$ and $\mathbf{2}^{2+}$, suggests that the new complexes may bind to DNA through a common mode. To investigate this question in more detail viscosity experiments were carried out.

Table 2. Summary of binding constant and binding site sizes obtained by UV-Visible titrations using complexes [**3**]Cl_4 and [**4**]Cl_4 and CT-DNA

Complex[a]	K_b /mol^{-1}dm^3	S /bp
$\mathbf{1}^{2+}$	8.8 x10^6	2.2
$\mathbf{2}^{2+}$	3.0 x 10^5	5.8
$\mathbf{3}^{4+}$	3.7 x 10^6	1.39
$\mathbf{4}^{4+}$	1.0 x 10^6	1.7

[a]Binding parameters for $\mathbf{1}^{2+}$ and $\mathbf{2}^{2+}$ previously reported in reference 27.

Relative viscosity studies.

Viscosity studies can readily identify binding modes to duplex DNA.[33] For example, since intercalation lengthens DNA, the relative viscosity of DNA solutions will go up on the introduction of intercalating substrates, whereas classical groove binders do not change DNA structure and thus have no effect on viscosity.[34-36] In this context, the addition of $\mathbf{3}^{4+}$ or $\mathbf{4}^{4+}$ to DNA solutions results in strikingly different viscosity changes.

In contrast to $\mathbf{1}^{2+}$ and $\mathbf{2}^{2+}$, which behave as typical intercalators, and only produce large increases in viscosity, surprisingly both $\mathbf{3}^{4+}$ and $\mathbf{4}^{4+}$, initially induce large *decreases* in the viscosity of the DNA solution – Figure 6. This is then followed by a steady increase in viscosity to levels seen for classical intercalators. Viscosity change in solutions of rigid rod-like DNA are proportional to changes in hydrodynamic length, therefore the observed decrease in viscosity at low binding ratios are indicative of large decreases in DNA contour lengths; while at higher binding ratios, DNA lengths roughly return to their original values.

Related viscosity changes have been observed when non-intercalating systems interact with DNA occur; indeed this data is similar to that observed for the interaction of multinuclear Ru^{II}/Re^{I} macrocycles with DNA. [20,34] In such cases, it is assumed that the decrease in hydrodynamic lengths is due to substrate-induced DNA bending and kinking which - as they increase in occurrence - produce rod-like super-helical structures

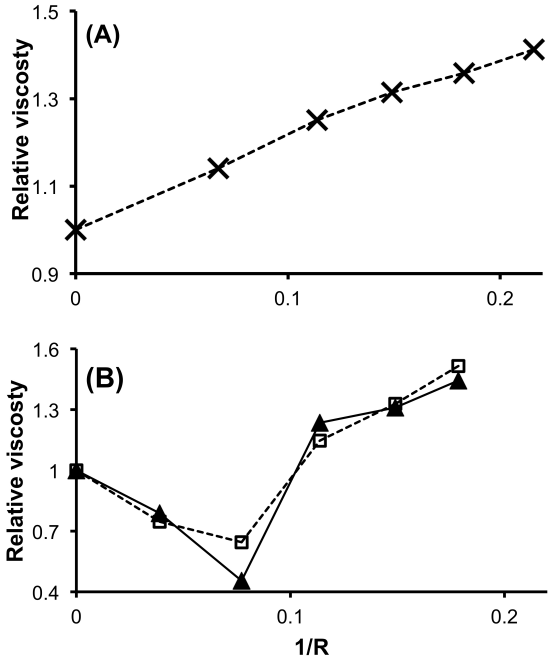

Fig 8 Changes in the relative viscosity of buffered DNA solutions on the addition of: (A) [**2**]Cl_2; (B) [**3**]Cl_4 and [**4**]Cl_4 in the same conditions (27 °C, 5 mM Tris buffer, 25 mM NaCl, pH 7, R=[DNA]/[ligand]).

The fact that $\mathbf{3}^{4+}$ and $\mathbf{4}^{4+}$ are groove binding is somewhat unexpected. Whilst dinuclear complexes of tpphz are established to be non-intercalating groove binders,[37,38] this is due to coordination of metal centres at both ends of the ligand preventing all but threading intercalation; similarly, the more extended [μ-bidppz $(bipy)_4Ru_2]^{4+}$ system, which incorporates the "face-to-face dppz bridging ligand, bidppz (11,11'-bis(di-pyrido[3,2-a :2',3'-c]phenazinyl), initially groove binds to duplex DNA.[39,40,41,42] As seen from the crystal structure, the terminal bipyridyldiylium group of the quaternized tpphz ligand does include a "propeller twisted" ethylene group that produces a slight deviation from complete planarity, but the steric demand of this structure is low and many conventional intercalators, such as ethidium bromide, ellipticine, and amasacrine, have bulkier groups attached to their intercalating surface. Indeed, given that they contain a large extended planar ligand, in many respects both $\mathbf{3}^{4+}$ and $\mathbf{4}^{4+}$ fulfil all the apparent structural prerequisites for classical intercalators. Apart from the added bipyridyldiylium group, the only major difference between the structurally related pairs of complexes is the increase in charge on $\mathbf{3}^{4+}$ and $\mathbf{4}^{4+}$ and it seems the preference for groove binding over intercalation can be attributed to these modifications.

It is well established that one of the main driving forces of groove binding is the interaction between cationic moieties on the binder and the negative charge of DNA, which is largely localized within its grooves. So, an increase in cationic charge within a system may increase the likelihood of groove binding. Indeed, a number of purely organic fused polyaromatic cations - that fit all the criteria for intercalation – have been discovered to be groove binders. For example studies on a series of substituted

anthraquinones show that intercalation switches to groove binding on moving from dicationic to tetracationic derivatives.[43] Moreover, previously reported rigid carbazole-based cations that groove bind[44,45] display some similarities, in structure and charge distribution, to the "long edge" of complexes $\mathbf{3}^{4+}$ and $\mathbf{4}^{4+}$ - Figure 7, which also matches the curvature of a DNA groove.

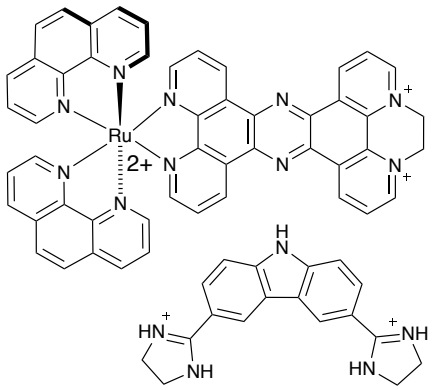

Figure 7. Comparison of the structure complex $\mathbf{4}^{4+}$ with a fused polyaromatic carbazole-based groove binder.

Conclusions

The new tetracationic complexes reported herein both possess a polyaromatic ligand with terminal bipyridyldiylium moiety. The extended flat surface of this quaternized tpphz ligand appears to be almost ideally suited to intercalation into duplex DNA, yet experimental studies show this assumption is incorrect. In fact - despite structural similarities - these systems have very different binding properties to their dicationic analogues, which are confirmed intercalators. In a previous study we have shown that metal complexes containing ligands with flexible, unfused aromatic ligands can still be intercalators; conversely, this study illustrates how the assumption that complexes with extended flat aromatic surfaces must to be intercalators is not always correct. These observations serve to reinforce previous caveats that DNA binding modes can only be ascertained through experiments that depend either on detecting modulations in the hydrodynamic properties of DNA or directly measuring mechanical changes in DNA -such as changes in average length of duplex structures.

The photochemical properties of the new complexes suggest that they may form the basis of novel light induced charge separation architectures or function as tools to investigate the effect of charge injection into DNA structures. Such studies will form the basis of future reports.

Experimental section

General methods

The ligand tpphz and complexes $\mathbf{1}^{2+}$ and $\mathbf{2}^{2+}$ were synthesized through reported procedures all other chemicals were purchased from commercial sources and were used as supplied unless otherwise stated. Cyclic voltammograms were recorded using an PAR VersaSTAT 4 potentiostat. Measurements were made using approximately 2mmol solution made up in freshly distilled acetonitrile containing 0.1M recrystallised Bu_4NPF_6 as the support electrolyte. Potentials were measured against an Ag/AgCl electrode.

Synthesis of $[3](PF_6)_4$

[1]$(PF_6)_2$ (0.20g) and dibromoethane were gently refluxed for 8 days under an argon atmosphere, which led the gradual formation of a dark brown precipitate. After cooling, the precipitate was filtered and collected. The resultant solid was dissolved in water (30 ml), and the solution filtered to remove any solid impurity. Ammonium hexafluorophosphate was added to the aqueous filtrate and the precipitate was collected. The solid was washed with water 50 ml and dried overnight *in vacuo*. Yield = 44 % (brown solid). ^{1}H NMR (d^3-acetonitrile): δ_H = 10.8 (d, 2H,J_{HH}=8.5 Hz,), 9.9 (dd, 2H,J_{HH}=8.2 Hz, 1.1Hz), 9.6 (d, 2H,J_{HH}=, 5.6 Hz), 8.9 (m, 2H), 8.68 (dd, 2H,J_{HH}=8.3Hz, 1.0Hz), 8.33(s, 2H) 8.27 (dd, 2H,J_{HH}=5.3 Hz, 1.1Hz) 8.08 (dd, 2H,J_{HH}=5.4 Hz, 1.2Hz,), 7.9 (m,4H), 7.78 (m, 4H), 5.64(s, 4H). TOF MS-ES; m/s (%)m/s (%) 582(40) $[M^{2+}$-2$(PF_6)/2]$, 339.8(35)$[M^{3+}$-3$(PF_6)/3]$. Acc.MS Calculated for $C_{46}H_{32}N_{10}RuP_2F_{12}/2$: [558.0570] Observed: 558.0572. C, 38.32; H, 2.52; N, 9.71. Observed: C, 38.32; H, 2.52; N, 9.38
Elemental Analysis calculated for $C_{46}H_{32}N_{10}RuP_4F_{24}.2H_2O$: C, 38.32; H, 2.52; N, 9.72. Observed: C, 38.36; H, 2.56; N, 9.38.

Synthesis of of $[3](PF_6)_4$

The synthesis of this complex was achieved using the same procedure used for $[\mathbf{3}](PF_6)_4$ but with $[\mathbf{2}](PF_6)_2$ (0.2g) as the starting material. Yield) = 0.11 g (39 %) brown solid. ^{1}H NMR (d^3-acetonitrile): δ_H =10.8 (dd, 2H,J_{HH}=8.4Hz, 1.1Hz), 10.0 (dd, 2H,J_{HH}=8.3 Hz, 1.2 Hz), 9.5(dd, 2H,J_{HH}=11.0 Hz, 1.0 Hz), 8.85(m, 2H), 8.60 (m, 6H), 8.33 (dd, 2H,J_{HH}=5.4 Hz, 1.2 Hz), 8.15 (m, 2H), 8.06 (m, 2H), 7.9 (d, 2H, J_{HH} = 4.9 Hz), 7.878 (d, 2H, J_{HH} = 5.1Hz), 7.5(m, 2H),7.2(m, 2H), 5.60(s, 4H). TOF MS-ES; m/s (%) 558(100)$[M^{+2}$-2$(PF_6)]$. Acc.MS Calculated for: $C_{50}H_{32}N_{10}RuP_2F_{12}$ /2: [582.0570] Observed: 582.0544.
Elemental Analysis calculated for $C_{50}H_{32}N_{10}RuP_4F_{24}$: C, 41.31; H, 2.22; N, 9.63. Observed: C, 40.97; H, 2.50; N, 9.65.

Computational Studies

Density functional theory (DFT) calculations were performed using Gaussian09, version D.01.[46] The B3LYP[47] functional was used throughout with the GD3-BJ correction[48] to account for dispersion interactions, whereby it is noted that in this case the correction did not significantly affect the results in comparison to the bare B3LYP functional. All calculations were performed using ultrafine integrals and with the 6-311G** basis set[49] on all C, N, H, and O. A Stuttgart-Dresden pseudopotential[50] was used on Ru throughout. This basis set/functional combination was found to give good correlation with experiment in previous work.[51-54] The starting atomic coordinates of all complexes were based on the crystal structure of $\mathbf{[3]}^{4+}$ reported above. After obtaining the minimum energy structures, we performed a single-point TD-DFT calculation to obtain excitation energies. All minima were confirmed to be true minima through the absence of imaginary frequencies in a subsequent frequency calculation. Hereby, we ignored any small imaginary frequencies (> -10 cm^{-1}), since they would have been caused by inaccuracies in the integration grid.
All calculations performed on these systems were done using acetonitrile as the solvent via a polarizable continuum model

(PCM)[55] using the standard parameters as supplied by Gaussian. Visualization was done by a in-house developed Python script for the TD-DFT spectra, Jmol[56] and Povray[57] for the geometries. Finally, supporting information was created using in-house developed software based on the OpenEye toolkit.[58] No symmetry was taken into account in our calculations.

Single Crystal X-ray Diffraction Studies

Intensity data was collected at 100 K on a Bruker SMART 1000 diffractometer operating with a MoKα sealed-tube X-ray source from crystals mounted in fomblin oil and cooled in a stream of cold N_2. Data were corrected for absorption using empirical methods (SADABS[59]) based upon symmetry equivalent reflections combined with measurements at different azimuthal angles[60]. The crystal structures were solved and refined against F^2 values using ShelXT[61] for solution and ShelXL[62] for refinement accessed *via* the Olex2 program[63]. Non-hydrogen atoms were refined anisotropically. Hydrogen atoms were placed in calculated positions with idealized geometries and then refined by employing a riding model and isotropic displacement parameters.

[a]*Department of Chemistry, University of Sheffield, Sheffield, S3 7HF, UK Tel: 44 114 222 9325; E-mail: james.thomas@sheffield.ac.uk*

[b]*current address Department of Chemistry, University of Misurata, Libya*

† Electronic Supplementary Information (ESI) available: [details of any supplementary information available should be included here]. See DOI: 10.1039/b000000x/

Acknowledgements

A license for the OpenEye tools, obtained *via* the free academic licensing program, is gratefully acknowledged. HSD is grateful to Government of Libya for funding.

1 M. J. Waring, *Annu. Rev. Biochem.*, 1981, **50**, 159–192.
2 L. A. Marky, J. G. Snyder, D. P. Remeta and K. J. Breslauer, *J. Biomol. Struct. Dyn.*, 1983, **1**, 487–507.
3 J. Feigon, W. A. Denny, W. Leupin and D. R. Kearns, *J. Med. Chem.*, 1984, **27**, 450–465.
4 D. E. Graves and L. M. Velea, *Current Organic Chemistry*, 2000, **4**, 915–929.
5 E. R. Jamieson and S. J. Lippard, *Chem. Rev.*, 1999, **99**, 2467–2498.
6 R. A. Alderden, M. D. Hall and T. W. Hambley, *J. Chem. Educ.*, 2006, **83**, 728–8.
7 V. Cepeda, M. A. Fuertes, J. Castilla, C. Alonso, C. Quevedo and J. M. Perez, *Anticancer Agents Med Chem*, 2007, **7**, 3–18.
8 C. Metcalfe and J. A. Thomas, *Chem Soc Rev*, 2003, **32**, 215–10.
9 *Dalton Trans*, 2007, 4903–4917.
10 M. Groessl and C. G. Hartinger, *Anal Bioanal Chem*, 2013, **405**, 1791–1808.
11 A. E. Friedman, J. C. Chambron, J. P. Sauvage, N. J. Turro and J. K. Barton, *J. Am. Chem. Soc.*, 1990, **112**, 4960–4962.
12 K. E. Erkkila, D. T. Odom and J. K. Barton, *Chem. Rev.*, 1999, **99**, 2777–2796.
13 A. W. McKinley, P. Lincoln and E. M. Tuite, *Coord Chem Rev*, 2011, **255**, 2676–2692.
14 M. R. Gill and J. A. Thomas, *Chem Soc Rev*, 2012, **41**, 3179–3192.
15 A. Notaro and G. Gasser, *Chem Soc Rev*, 2017, **46**, 1–21.
16 F. E. Poynton, S. A. Bright, S. Blasco, D. C. Williams, J. M. Kelly and T. Gunnlaugsson, *Chem Soc Rev*, 2017, **36**, 1–51.
17 L. Zeng, P. Gupta, Y. Chen, E. Wang, L. Ji, H. Chao and Z.-S. Chen, *Chem Soc Rev*, 2017, **46**, 5771–5804.
18 A. Ghosh, P. Das, M. R. Gill, P. Kar, M. G. Walker, J. A. Thomas and A. Das, *Chem. Eur. J.*, 2011, **17**, 2089–2098.
19 V. Ramu, M. R. Gill, P. J. Jarman, D. Turton, J. A. Thomas, A. Das and C. Smythe, *Chem. Eur. J.*, 2015, **21**, 9185–9197.
20 D. Ghosh, H. Ahmad and J. A Thomas, *Chem. Commun.*, 2009, 2947–2949.
21 H. Ahmad, D. Ghosh and J. A. Thomas, *Chem. Commun.*, 2014, **50**, 3859–3861.
22 M. G. Walker, P. J. Jarman, M. R. Gill, X. Tian, H. Ahmad, P. A. N. Reddy, L. McKenzie, J. A. Weinstein, A. J. H. M. Meijer, G. Battaglia, C. G. W. Smythe and J. A. Thomas, *Chem. Eur. J.*, 2016, **22**, 5996–6000.
23 H. Ahmad, A. Wragg, W. Cullen, C. Wombwell, A. J. H. M. Meijer and J. A. Thomas, *Chem. Eur. J.*, 2014, **20**, 3089–3096.
24 T. Phillips, I. Haq, A. J. H. M. Meijer, H. Adams, I. Soutar, L. Swanson, M. J. Sykes and J. A. Thomas, *Biochemistry*, 2004, **43**, 13657–13665.
25 T. Phillips, C. Rajput, L. Twyman, I. Haq and J. A. Thomas, *Chem. Commun.*, 2005, 4327–4329.
26 J. Bolger, A. Gourdon, E. N. Ishow and J.-P. Launay, *J. Chem. Soc., Chem. Commun.*, 1995, 1799.
27 M. R. Gill, H. Derrat, C. G. W. Smythe, G. Battaglia and J. A. Thomas, *Chembiochem*, 2011, **12**, 877–880.
28 J. Bolger, A. Gourdon, E. Ishow and J.-P. Launay, *Inorg Chem*, 1996, **35**, 2937–2944.
29 J. E. Dickeson and L. A. Summers, *Aust. J. Chem.*, 1970, **23**, 1023–1027.
30 M. R. Gill, P. J. Jarman, S. Halder, M. G. Walker, H. K. Saeed, J. A. Thomas, C. Smythe, K. Ramadan and K. A. Vallis, *Chem. Sci.*, 2018, **9**, 841–849.
31 J. D. J. McGhee and P. H. P. von Hippel, *J. Mol. Biol.*, 1974, **86**, 469–489.
32 R. B. Nair, E. S. Teng, S. L. Kirkland and C. J. Murphy, *Inorg Chem*, 1998, **37**, 139–141.
33 G. Cohen and H. Eisenberg, *Biopolymers*, 1969, **8**, 45–55.
34 S. Satyanarayana, J. C. Dabrowiak and J. B. Chaires, *Biochemistry*, 1992, **31**, 9319–9324.
35 D. Suh and J. B. Chaires, *Bioorganic & Medicinal Chemistry*, 1995, **3**, 723–728.
36 C. Metcalfe, C. Rajput and J. A. Thomas, *J. Inorg. Biochem.*, 2006, **100**, 1314–1319.
37 C. Rajput, R. Rutkaite, L. Swanson, I. Haq and J. A. Thomas, *Chem. Eur. J.*, 2006, **12**, 4611–4619.
38 D. A. Lutterman, A. Chouai, Y. Liu, Y. Sun, C. D. Stewart, K. R. Dunbar and C. Turro, *J. Am. Chem. Soc.*, 2008, **130**, 1163–1170.
39 P. Lincoln and B. Nord n, *Chem. Commun.*, 1996, 2145.
40 L. M. Wilhelmsson, F. Westerlund, P. Lincoln and B. Nordén, *J. Am. Chem. Soc.*, 2002, **124**, 12092–12093.
41 L. Wu, A. Reymer, C. Persson, K. Kazimierczuk, T. Brown, P. Lincoln, B. Nordén and M. Billeter, *Chem. Eur. J.*, 2013, **19**, 5401–5410.
42 A. A. Almaqwashi, J. Andersson, P. Lincoln, I. Rouzina, F. Westerlund and M. C. Williams, *Sci. Rep.*, 2016, **6**, 1–11.
43 D. T. D. Breslin, C. C. Yu, D. D. Ly and G. B. G. Schuster, *Biochemistry*, 1997, **36**, 10463–10473.
44 F. A. Tanious, D. Ding, D. A. Patrick, R. R. Tidwell and W. D. Wilson, *Biochemistry*, 1997, **36**, 15315–15325.
45 N. Dias, U. Jacquemard, B. Baldeyrou, C. Tardy, A. Lansiaux, P. Colson, F. Tanious, W. D. Wilson, S. Routier, J.-Y. Mérour and C. Bailly, *Biochemistry*, 2004, **43**, 15169–15178.
46. Gaussian 09, Revision D.01, M. J. Frisch, G. W. Trucks, H. B. Schlegel, G. E. Scuseria, M. A. Robb, J. R. Cheeseman, G. Scalmani, V. Barone, B. Mennucci, G. A. Petersson, H. Nakatsuji, M. Caricato, X. Li, H. P. Hratchian, A. F. Izmaylov, J. Bloino, G. Zheng, J. L. Sonnenberg, M. Hada, M. Ehara, K. Toyota, R. Fukuda, J. Hasegawa, M. Ishida, T. Nakajima, Y. Honda, O. Kitao, H. Nakai, T. Vreven, J. A. Montgomery, Jr., J. E. Peralta, F. Ogliaro, M. Bearpark, J. J. Heyd, E. Brothers, K. N. Kudin, V. N. Staroverov, R. Kobayashi, J. Normand, K. Raghavachari, A. Rendell, J. C. Burant, S. S. Iyengar, J. Tomasi, M. Cossi, N. Rega, J. M. Millam, M. Klene, J. E. Knox, J. B. Cross, V. Bakken, C. Adamo, J. Jaramillo, R. Gomperts, R. E. Stratmann, O. Yazyev, A. J. Austin, R. Cammi, C. Pomelli, J. W. Ochterski, R. L. Martin, K. Morokuma, V. G. Zakrzewski, G. A.

Voth, P. Salvador, J. J. Dannenberg, S. Dapprich, A. D. Daniels, O □. Farkas, J. B. Foresman, J. V. Ortiz, J. Cioslowski, and D. J. Fox, Gaussian, Inc., Wallingford CT, 2009.
47. A. D. Becke. J. Chem. Phys. 98, 5648 (1993).
48. S. Grimme, S. Ehrlich, and L. Goerigk, *J. Comp. Chem*. **32** (2011) 1456-65.
49. A. D. McLean, G. S. Chandler. J. Chem. Phys. 72, 5639 (1980); R. Krishnan, J. S. Binkley, R. Seeger, J. A. Pople. J. Chem. Phys. 72, 650 (1980).
50. X. Y. Cao, M. Dolg. J. Chem. Phys. 115, 7348 (2001); A. Nicklass, M. Dolg, H. Stoll, H. Preuss. J. Chem. Phys. 102, 8942 (1995).
51. H. Ahmed, A. J. H. M. Meijer, J. A. Thomas, Chem. Asian J. 6, 2339 (2011).
52. S. P. Foxon, C. Green, M. Walker, A. Wragg, H. Adams, J. A. Weinstein, S. C. Parker, A. J. H. M. Meijer, J. A. Thomas, Inorg. Chem. 51, 463 (2012); Jonathan Best, Igor V. Sazanovich, Harry Adams, Robert D. Bennett, E. S. Davies, Anthony J. H. M. Meijer, M. Towrie, S. A. Tikhomirov, O. V. Bouganov, Michael D. Ward and Julia A. Weinstein, Inorg Chem, 49, 10041 (2011).
53. P. Waywell, V. Gonzalez, M. R. Gill, H. Adams, A. J. H. M. Meijer, M. P. Williamson, J. A. Thomas, Chem. Eur. J., 16, 2407 (2010)
54. Michael G. Walker, Vadde Ramu, Anthony J. H. M. Meijer, Amitava Das, and Jim A. Thomas, Dalton Trans., **46**, 6079-6086 (2017)
55. B. Mennucci, J. Tomassi. J. Chem. Phys. 106, 5151 (1997); M. Cossi, V. Barone, B. Menucci, J. Tomassi. Chem. Phys. Lett. 286, 253 (1998).
56. Jmol: an open-source Java viewer for chemical structures in 3D. http://www.jmol.org/ [last accesssed: 9 Jun 2017].
57. Persistence of Vision Pty. Ltd. (2004). Persistence of Vision (TM) Raytracer. Persistence of Vision Pty. Ltd., Williamstown, Victoria, Australia. http://www.povray.org/ [Last accessed: 9 Jun 2017].
58. OEChem, version 2.1.0, OpenEye Scientific Software, Inc., Santa Fe, NM, USA, www.eyesopen.com, 2016 [Last accessed: 9 Jun. 17]; J.A. Grant, J.A. Haigh, B.T. Pickup, A. Nicholls and R.A. Sayle, J. Chem. Inf. Model., 46, 1912 (2006).
59 Bruker (2016), SADABS. Bruker Axs Inc., Madison, Wisconsin, USA
60 L. Krause, R. Herbst-Irmer, G. M. Sheldrick & D. Stalke, *J. Appl. Cryst.,* 2015, **48**, 3–10.
61 G. M. Sheldrick, *Acta Cryst*., 2008, **A64**, 112-122.
62 G. M. Sheldrick, *Acta Cryst.*, 2015, **C71**, 3-8.
63 O. V. Dolomanov, L. J. Bourhis, R. J. Gildea, J. A. K. Howard, H. Puschmann, *J. Appl. Cryst.*, 2009, **42**, 339-341